Leveraging High-Density EMG to Investigate Bipolar Electrode Placement for Gait Prediction Models

Balint K. Hodossy [ID], Annika S. Guez [ID], Shibo Jing [ID], Weiguang Huo [ID], Ravi Vaidyanathan [ID], and Dario Farina [ID], *Fellow, IEEE*

Abstract— To control wearable robotic systems, it is critical to obtain a prediction of the user's motion intent with high accuracy. Surface electromyography (sEMG) recordings have often been used as inputs for these devices, however bipolar sEMG electrodes are highly sensitive to their location. Positional shifts of electrodes after training gait prediction models can therefore result in severe performance degradation. This study uses high-density sEMG (HD-sEMG) electrodes to simulate various bipolar electrode signals from four leg muscles during steady-state walking. The bipolar signals were ranked based on the consistency of the corresponding sEMG envelope's activity and timing across gait cycles. The locations were then compared by evaluating the performance of an offline temporal convolutional network (TCN) that mapped sEMG signals to knee angles. The results showed that electrode locations with consistent sEMG envelopes resulted in greater prediction accuracy compared to hand-aligned placements ($p < 0.01$). However, performance gains through this process were limited, and did not resolve the position shift issue. Instead of training a model for a single location, we showed that randomly sampling bipolar combinations across the HD-sEMG grid during training mitigated this effect. Models trained with this method generalized over all positions, and achieved 70% less prediction error than location specific models over the entire area of the grid. Therefore, the use of HD-sEMG grids to build training datasets could enable the development of models robust to spatial variations, and reduce the impact of muscle-specific electrode placement on accuracy.

Index Terms—Artificial intelligence (AI) and machine learning, human–robot interaction, rehabilitation robotics, sensor networks, signal processing.

I. Introduction

EXOSKELETONS and other wearable robotic devices are designed to guide and support users in a variety of contexts, from rehabilitation to movement augmentation. In most cases, a user-driven human–machine control interface is necessary to ensure active participation from the user [1]. By estimating the active contribution of the subject to the desired motion, an exoskeleton can provide the required level of assistance synchronously with the user's movement—i.e., assist-as-needed (AAN) control [2], [3]. The performance of the system therefore depends on the reliability of the signals used as inputs to the model that estimates the intended motion.

Surface electromyography (sEMG) is a commonly used non-invasive sensing modality for motion intent estimation due to inherent association between muscle signals and movement [4]. A subject's sEMG signals can be used as indicators of voluntary effort [5] and as inputs for gait prediction models [6], [7], which form key elements in the control schemes of wearable robotics [8].

Despite the extensive use of sEMG in human–machine interfacing and clinical practice [9], there is a limited number of studies that assess the impact of electrode shift for lower limb assistive devices [10], especially when employing deep learning methods [11]. Whilst some studies have investigated the effect of electrode placement on signal characteristics for lower-limbs [12], this has not been done across different signal acquisition and gait conditions, such as wearing an orthosis. Furthermore, changes in electrode location can cause significant distortions in the EMG signal features required for pattern recognition [13], making previously learnt features inapplicable unless the model is retrained or calibrated for the new location [7].

Based on the signal's sensitivity to electrode placement, there are the following two main approaches that have the potential to mitigate this effect and help the model retain high gait prediction accuracy.

1) Determine the electrode location on each muscle that will provide the highest sEMG signal quality.
2) Develop a model that is robust across electrode locations.

While available standards and tutorials [14], [15] provide some indication on sEMG electrode placement, these are unspecific and often do not account for the signal variability during dynamic movements [12], [16], [17], or the changes introduced by donning an orthosis with limited degree of freedoms (DoFs).

Furthermore, there is no guarantee that these palpation- and eyesight-based guidelines provide the location of the optimal signal for pattern recognition-based control schemes [18].

Previous studies have attempted to mitigate the impact of electrode shifts by including additional preemptive steps that recognise and compensate for them. These are either signal registration methods transforming signals to a predetermined expected distribution [19], or conversely apply the appropriate prediction model from an ensemble [20], [21]. Alternatively, models can be trained on a distribution of locations simultaneously, either recorded experimentally [22] or simulated through data augmentation [23].

In this study, we investigated both methods (selection of electrode location and generalization of the model by extended training), and compared their usability in practice. For this purpose, we used temporal convolutional networks (TCNs) as an example of a data-driven model suited to regress time-series data [24]. This network architecture benefits from more straightforward implementation and much faster training times than its recurrent counterparts, while maintaining comparable performance [25]. Previously, TCNs have been successfully applied to lower limb exoskeleton control with inertial sensor data [26], [27], and recently for bipolar sEMG-based control [28]. Here, single channel bipolar sEMG signals were used to estimate the knee angle in a one-step-ahead offline prediction scheme. Muscle signals were sampled from grids placed on knee and ankle flexor and extensor muscles.

To compare a wide range of bipolar electrode placements, high-density surface electromyography (HD-sEMG) grids were used to simultaneously acquire data from a larger surface area of the skin, which allowed sampling of bipolar signals from various positions and orientations [29]. This diverse dataset was then used to produce more reliable convolutional models for exoskeleton applications under dynamic conditions, and was also tested when a one-DOF passive orthosis was donned. The orthosis condition was not investigated in an attempt to model a patient user. Instead, it was used to examine whether signal artefacts from the DoF restriction or the orthosis' contact with grid impact the performance of our models. While the device used here was passive, noise from these sources is expected to be similar in an actuated rigid exoskeleton as well. In addition to our use of location specific models to evaluate signal quality, we showed that TCNs are capable of learning features suitable for robust prediction across the area of the grid. This is achieved by randomly sampling bipolar electrode location during training. This technique is a promising method for mitigating the effect of electrode shift on deep learning models. Our findings highlight the potential of using the spatial information from HD-sEMG data to improve model robustness for bipolar signal driven control applications.

II. MATERIALS AND METHODS

A. Subjects

Five subjects (three male, two female, mean age $= 25 \pm 4$ years) were chosen for this study, with no history of neurological or physiological conditions that could impact their natural gait.
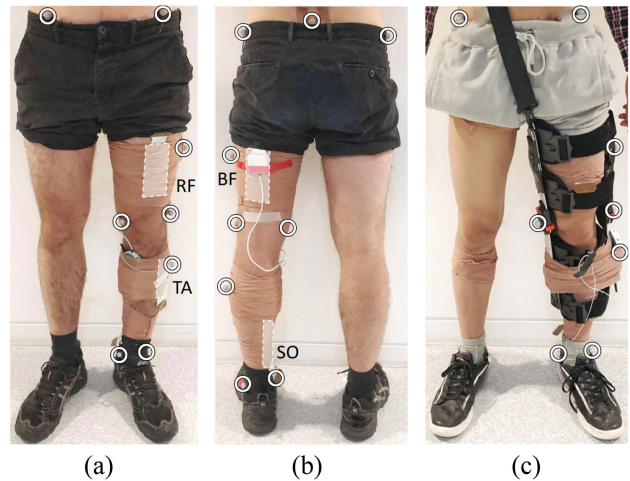

Fig. 1. Experimental setup, showing the HD-sEMG grid placements (white rectangles) (a) the RF and TA, (b) the BF and SO, the motion capture marker positions (white circles). (c) Set-up with the passive orthosis strapped to the subject's leg.

Informed consent was obtained for all subjects. The experiments for data acquisition were performed in compliance to ethical documentations approved by the Imperial College Research Ethics Committee (ICREC reference: 21IC7204).

B. Experimental Setup

1) High-Density Surface Electromyography: For all subjects, HD-sEMG signals were recorded independently from the Rectus Femoris (RF), the Biceps Femoris (BF), the Tibialis Anterior (TA), and the Soleus (SO) using 13×5 electrode grids in monopolar derivation (eight-mm interelectrode spacing; model number GR08MM1305). When recording, the relevant grid was connected to a Sessantaquattro acquisition system, and the ground electrode was placed on the same leg's lateral malleolus, using a designated damp ankle strap. All equipment used for the acquisition of the HD-sEMG data came from OT Bioelettronica, Italy [30].

The positioning of the centres of the electrode grids followed the SENIAM placement guides [14]. Throughout the article, any mention of the "middle" or "standard" sampling will refer to the bipolar placement following SENIAM standards.

A double-sided adhesive foam (model number FOA08MM1305) was placed on the HD-sEMG grid, and CC1 ac conductive cream was applied to the grid to ensure satisfactory contact between the electrodes and the skin. Before electrode placement, the area of skin was shaved as needed, mildly abraded with abrasive paste, cleansed with a nonirritating alcoholic solution, and dried.

2) Motion Capture: The knee joint kinematics were acquired using a Vicon Motion Capture system equipped with ten 120 Hz Vicon Vero v2.2 cameras placed around the treadmill, mounted on the ceiling of the recording space. Trajectory data were labeled and gap-filled in Vicon Nexus.

Rigid body segments were reconstructed using the following set of markers (see Fig. 1).

1) *Pelvis:* Two markers placed on the superficial aspects of the left and right anterior superior iliac spines (ASISs), and one marker on the sacrum.
2) *Thigh:* Two markers placed on the femoral epicondyles, and one marker placed on the lateral side of the thigh.
3) *Shank:* Two markers placed on the lateral and medial malleoli, and one marker placed on the lateral side of the shank.

Knee flexion was defined according to [31] using all above-mentioned segments. The hip joint centre was approximated as a fixed position in the pelvis' coordinate frame, scaled by the ASIS breadth [32].

When wearing the passive orthosis (see Fig. 1), the lateral thigh and shank markers were replaced onto the orthotic frame after all other components had been fitted. Both the medial and lateral epicondyle markers were placed along the axis of rotation of the orthosis. The HD-sEMG grids were not moved or replaced when donning the knee brace.

3) System Synchronization: Shared reference pulses, sent from a microcontroller at the start and end of a trial, were recorded by both data acquisition systems. These were then used in the preprocessing phase to methodically align the sEMG and motion capture signals in time based on the timing of the rising edges of the pulses.

C. Experimental Procedure

Each subject was asked to walk on a treadmill at a steady-state speed of 0.8 m/s, selected to be comfortable for all subjects. Two three-minute trials were recorded for each muscle separately, with rest breaks in-between to ensure muscle fatigue would not impact the recordings. This led to a total of 40 recorded steady-state trials (two trials $\times$ four muscles $\times$ five subjects), with approximately 350–400 strides per trial. For the second half of the experimental session, the user was fitted with a dual-hinged, single DoF passive knee support brace. A single two-minute trial was recorded for each subject and muscle, leading to a total of 20 trials with the orthosis.

D. Signal Preprocessing

Bipolar signals were extracted from the 64 channel HD-sEMG grid by taking the monopolar voltage difference between an electrode and its neighboring electrodes within a three-electrode radius and a maximum angle from the longitudinal axis of $45°$ (see Fig. 2). This process was repeated for every electrode, and repeated pairings of electrodes were ignored. A total of 360 unique bipolar combinations that would satisfy these requirements for sensor placement contained within the grid were identified.

The motion capture data were up-sampled to the EMG sampling frequency (2000 Hz) using linear interpolation, and the data were cropped to extract the steady-state walking sequence.

The consistency metric analysis was performed based on the sEMG envelope. To obtain it, the signals were digitally band-pass filtered (fourth order Butterworth, 20–400 Hz), rectified, and subjected to a ten Hz low-pass filter. gait cycles (GCs) were segmented using the peak angles of the knee, and temporally
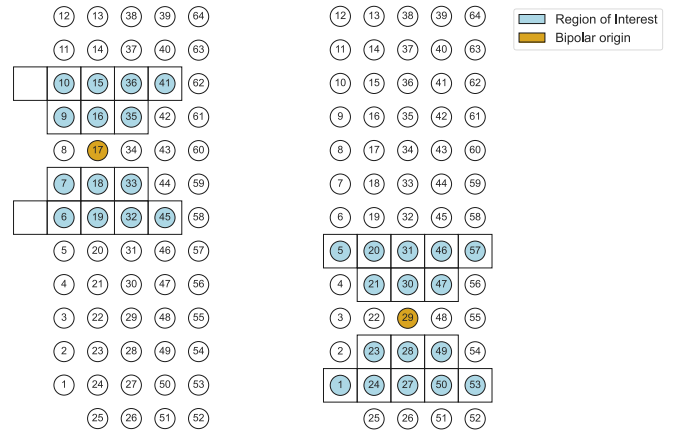

Fig. 2. Range of neighboring electrodes considered for each electrode when determining the bipolar combinations. This schematic shows the combinations extracted for two example electrodes. The "origin" electrode (orange) was eligible for pairing with all the electrodes (blue) from its region of interest. This resulted in up to 16 possible bipolar combinations for each electrode.

normalized so that one GC corresponded to 100% of the time axis.

During preprocessing stages, two HD-sEMG files were found corrupted and were excluded from further analyses, reducing the dataset from 40 available trials to 38. The remaining data still covered all subjects and muscles investigated due to repeated trials.

E. Bipolar Sampling Selection

Quantifying a single bipolar channel's quality by training a location specific TCN model takes several hours. This gives motivation for identifying quick-to-evaluate metrics that indicate suitability for regression. We selected channels to evaluate with TCN performance based on metrics of sEMG envelope consistency. While most studies focus on the location with sEMG maximum amplitude [33], [34], this study investigated the consistency of the signal across steady-state gait cycles as a measure of quality [12]. Considering how many myoelectric control models are based on pattern recognition mechanisms, it was hypothesized that a consistent signal would lead to more accurate and stable predictions.

The consistency across gait cycles was calculated from the following three measures of signal's envelope:
1) maximum peak amplitude;
2) integrated area;
3) the gait phase of the maximum peak's location.

For the first two of these metrics, the inverse of the coefficient of variation (CoV) was used to quantify the consistency of muscle patterns across the gait cycle (a lower CoV implied a higher consistency), expressed as the standard deviation (σ) normalized by the cycle's mean value (μ) and given in percentage form

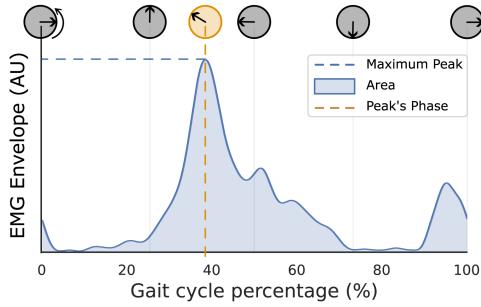$$\mathrm{CoV}(\%) = \frac{\sigma}{\mu} \times 100. \tag{1}$$

Fig. 3. Illustration of the three envelope measures within a gait cycle that were used to quantify signal consistency for the RF. Channels are considered more consistent if these measures do not change from cycle to cycle. Phasor representation of the continuous progress along gait cycle is shown above the curve.

The location of the maximum sEMG peak within the gait cycle was expressed using phasor representation calculated by

$$\Phi_t = \left(e^{j2\pi/T}\right)^t \qquad t \in [0, T-1] \cap \mathbb{Z} \qquad (2)$$

where t is the temporal index of the peak within a gait cycle of length T. This allows description of normalized progress in the gait cycle without discontinuity between the start and end. The average vector was calculated across all cycles and the variance metric was calculated using the absolute value of the angle between the peak location vector and the normalized average vector. An illustration of the measures used to quantify consistency is shown on Fig. 3.

The electrode channels were ordered with ascending variation of the three metrics to facilitate the selection of those with the least variation (i.e., the most consistent ones), or conversely the ones with the highest variability (i.e., least consistent). Evaluating all three metrics for our entire dataset took less than two minutes. However, the obtained rankings were different across all three consistency metrics.

To resolve this issue, we employed a method that combined the channel selections of all three metrics, referred to as the *Agreement* approach. This procedure consisted of selecting the first bipolar electrode combination that occurred across all metrics when progressing through their respective ordered consistency rankings. This ensured all three metrics were considered when selecting the electrode pair. On average, a match was found in the first 10% of the ranked combinations.

To determine whether to rely on one of the three rankings or the Agreement approach, preliminary tests were conducted where one TCNs model was trained and evaluated with a 50-50 train-validation split for three subjects, across every muscle with each sampling method. From the results shown in Fig. 4, the Agreement approach was subsequently adopted for all following evaluations as its chosen sampling led to the highest model performance.

A common bipolar electrode size (64 mm^2) was simulated virtually by spatially filtering the HD-sEMG grid with a 2×2 averaging window before sampling bipolar signals, reducing the grid size from 13×5 electrodes to 12×4. No significant difference in model output was observed, so remaining experiments were conducted with the HD-sEMG signals to allow
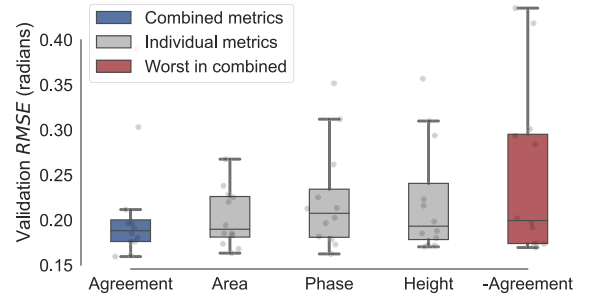

Fig. 4. Metric selection for further analysis based on model performance on reduced dataset. Angle prediction error on validation data is compared for one model trained for each muscle of the first three subjects. The labels for each plot correspond to the metric used to determine the channel locations for that group's TCNs. The "-Agreement" label specifies the least consistent electrode location based on the "Agreement" method.
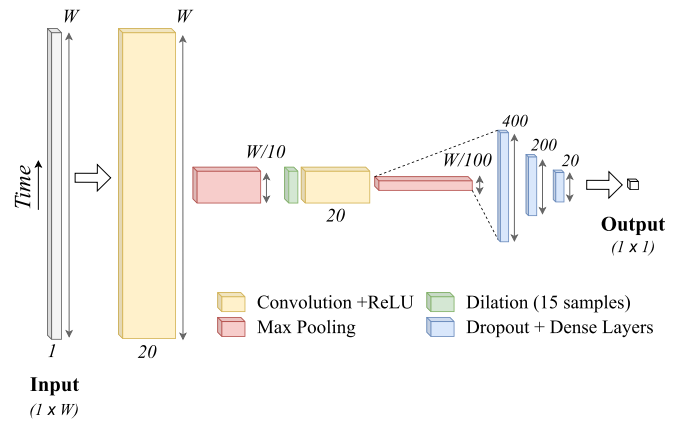

Fig. 5. Schematic of the 1-D TCN architecture, mapping the windowed sEMG signal ($1 \times W$) to the user's knee angle (1×1). W stands for the width of the input window, either 1000 or 500 samples.

the inclusion of samplings with smaller interelectrode distance (IED) as well (8 mm).

F. Knee Angle Prediction Model

The TCNs investigated were composed of two convolutional layers with pooling and dilation layers between them. This was followed by three dense layers with dropout in-between (see Fig. 5). This architecture is similar to the one in [35].

No envelope or other feature extraction was performed on the muscle signals, and no temporal normalization was applied. The sEMG input was normalized using the mean and standard deviation values from the entire training set of the given channel. Then, it was split into windows of equal sizes, partly overlapping at a 40 sample stride. Two window sizes were investigated, 500 and 1000 samples. The shorter (250 ms) window is similar to window lengths from TCNs used for EMG processing in upper limb contexts [36]. However, when compared to the upper limb tasks, gait is a more auto-correlated process. Therefore, a longer window (500 ms) was also explored. The windows were paired with the flexion signal in a one-step-ahead regression scheme. An early termination condition was used to stop training after 100 repeats of the training data, or after performance on

validation data has not improved or has worsened for the most recent six repeats.

1) Connection Between Consistency Metrics and Model Performance: Root Mean Square (RMS) error between the knee angle predicted by the model and the angle from the motion capture was calculated. The error of trained models on validation data was compared across different spatial sampling conditions and window sizes (250 ms and 500 ms). A five-fold split was performed on each training set for cross-validation [37], performed for each muscle and subject. The splitting of the recordings remained consistent across conditions, and no window was allowed in a fold of cross-validation that had any overlap with other folds. With five subjects, four muscles, and five folds, 100 models were trained and evaluated for each condition on spatial sampling and window size, for a total of 600 models in this comparison. The following bipolar channel selection methods were compared.

1) The subject and muscle specific channel with the best cross-metric consistency based on the Agreement approach, as outlined in Section II-E.
2) The bipolar combination aligned according to the SENIAM placement standard (between electrodes 31 and 33).
3) The subject and muscle specific channel with the worst cross-metric consistency based on the Agreement approach, as outlined in Section II-E.

2) Spatially Robust Bipolar Feature Learning: Models trained on the electrode combination in the middle (electrodes 31 and 33) were evaluated on the signals of all other valid electrode combinations. Their performance was compared with nonplacement specific models, which regressed signals from any valid combination in the grid directly. During the training of these TCNs, the bipolar channel that determines the signal was sampled uniformly from the set of all valid bipolar channels for each 500 ms input window. Therefore, even in this case, only a single channel of sEMG input was used at a time. To achieve consistent performance, the model needs to extract features that were suitable for generalizing over the area covered by the grid, and cannot optimize for any single placement. As such, this method can be considered as a technique for implicit regularization of sEMG models. Lastly, this analysis of model robustness to placement shifts was repeated while wearing a one-DoF knee orthosis, to simulate the impact an exoskeleton frame may have on the signal distribution due to restrictions to the range of motion or motion artefacts [38], [39]. A causal band-pass filter of 10–400 Hz was used, a common strategy to mitigate the impact of these types of interference [40]. This preprocessing was also applied for the models without the orthosis in this section, for a fairer comparison.

Performance was evaluated similarly to the previous section. For each training condition (training with a single location, or randomly sample during training) and orthosis condition (donned or doffed) a TCN is trained for each of the five subjects, four muscles, and five folds (100 for each condition).

The discussed methods of bipolar signal sampling from grids could potentially be used in clinical applications. Robust features may be learnt from HD-sEMG grid data, and then deployed

TABLE I
MEDIAN VALIDATION RMS ERROR AND STANDARD DEVIATION (σ) FOR 100
MODELS TRAINED ACROSS SUBJECTS AND MUSCLES

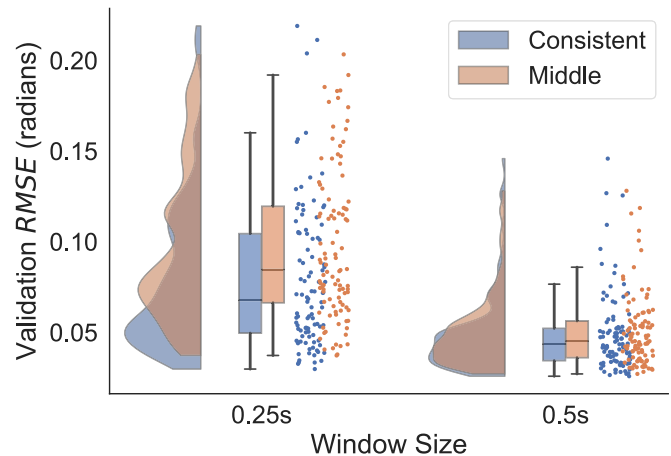| Channel selection	0.25 s	0.5 s
High consistency	0.067 ± 0.040	0.043 ± 0.022
Middle	0.084 ± 0.042	0.045 ± 0.020
Low consistency	0.084 ± 0.059	0.045 ± 0.028

Values in radian.

Fig. 6.   RMS error of angle predictions from TCNs trained on the combination with the best consistency score (blue) versus the middle electrode combination (orange), for two different input window durations. The kernel density, the box plot, and the raw data are shown for the different conditions.

with more convenient to use traditional bipolar sEMG signal acquisition devices. A preliminary data collection using a Delsys Trigno electrode system with two of the subjects was used to trial this approach. TCNs trained with bipolar signals from the HD-sEMG grid were applied to the acquired Delsys data (see Fig. 11 and Fig. 13).

Deep learning was performed using the Keras framework for TensorFlow [41], on a single computer with a Intel i7 CPU and NVIDIA GeForce 2070 GPU, taking less than 30 minutes to train a model.

III. RESULTS

A. Connection Between Consistency Metrics and Model Performance

The samplings chosen based on their score from the consistency metrics led to higher performance of the TCN, with a significantly lower validation Root Mean Squared Error (RMSE) compared to the bipolar location based on SENIAM standards and inconsistent samplings (see Table I which summarizes the median and σ statistics). This validates the metrics as indicators of signal quality, suggesting they could be used as a preliminary verification method for sEMG-based models, whilst also demonstrating the impact of electrode placement for sEMG pattern recognition.

Fig. 6 shows the validation RMS flexion angle prediction error distributions of models of different electrode locations and

Training channels	No orthosis	orthosis
Full grid	0.090 ± 0.030	0.122 ± 0.044
Middle only	0.309 ± 0.096	0.338 ± 0.109

Fig. 7. Visualization of the average cross-cycle values of the sEMG envelopes' (a) integrated area, (b) maximum peak amplitude, and (c) maximum peak location in terms of GC percentage (with 0% corresponding to the heel strike) for a subject's SO (1) without and (2) with the orthosis. Each of the graphs show the spatial distribution of the metrics across the HD-sEMG grid, and the values shown correspond to the vertical differential between two monopolar electrodes (therefore showing a 12×5 grid as opposed to the original 13×5 monopolar grid.

input window sizes. The use of a larger window size can help mitigate the effect of electrode position (see Fig. 6). This comes at additional computational costs, which may be important considerations for real-time applications.

The prediction error was comparable to other gait regressors reported in the literature [11]. Due to the non-Gaussian distribution, and to take intersubject variation into account, paired nonparametric tests were used to assess differences and interactions between groups. A Friedman test showed significant differences in distributions, $p << 0.0001$, which was mostly due to differences across window sizes.

When repeating the test within the shorter window groups, differences remained significant ($p = 0.0263$), therefore further intergroup comparisons were made. The hypothesis that samplings with high consistency scores perform better than the sampling from the middle was tested with a one-tailed Wilcoxon signed-rank test. The "consistent" sampling has a lower mean error of the two with $p = 0.0002$. Similarly, models using the "consistent" sampling had a lower error than those trained with "inconsistent" signals ($p = 0.010$).

When repeating the Friedman test within the longer window groups, no significant differences in RMS error was detected ($p = 0.432$).

B. Effect of the Orthosis on the sEMG Recorded Signals

Even though the bipolar locations with high consistency scores performed better, this optimal placement selected during normal walking did not transfer when donning the orthosis, as the muscle activation patterns showed significant changes in amplitude and spatial distribution across these two conditions.

Fig. 7 illustrates the change in behavior of the three metrics when comparing the muscle activation patterns across the grid with and without the orthosis. Whilst some features seem to have some spatial similarities across conditions, the amount of muscle activity (shown by the envelope's integrated area) and the peak activation amplitude intensify when wearing the orthosis, and become significant in areas of the muscle that were initially inactive. In addition, the main activation peak takes place earlier in the gait cycle around the belly of the muscle, further distorting the pattern the model was trained on. This behavior is in conflict with the hypothesis that there exists a subject-specific area on each muscle that will consistently provide reliable muscle activation patterns and generalize across conditions such as donning an orthosis.
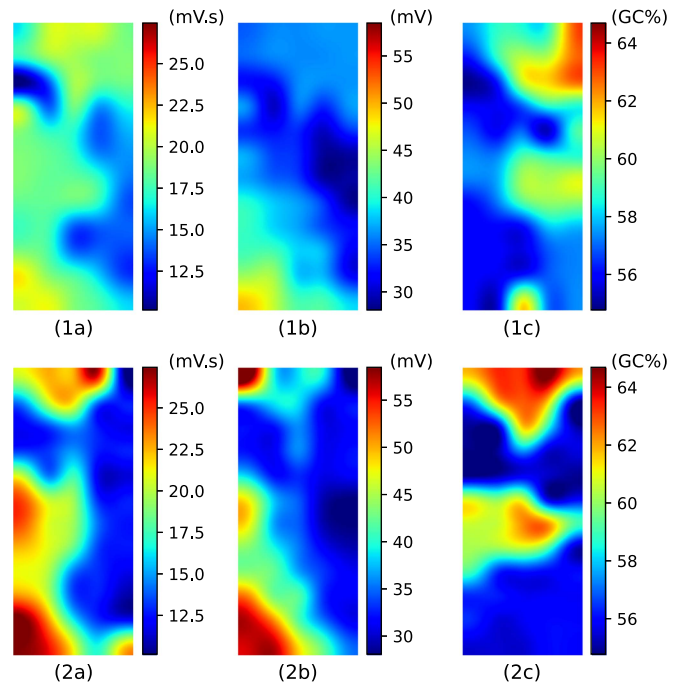
C. Spatially Robust Regression With Location Sampling

Table II and Fig. 10 evaluate the capability of the TCN to generalize over the available electrode combinations on the grid when compared to a single location training. There was a significant drop in validation RMSE when training the model with all the possible bipolar combinations contained within the HD-sEMG grid. A Friedman test was used for the four conditions to evaluate the capacity for the model to generalize, and the improvements in performance across all conditions were significant with Wilcoxon signed-rank tests at $p < 0.01$. Fig. 12 further illustrates the increased robustness of the gait prediction model, with a significantly lower σ across different electrode combinations.

Fig. 9 shows the four conditions investigated in Fig. 10, with model performance scores separated based on which muscle they were trained on. The relationships between the median RMS error from different muscle inputs is unchanged between conditions, with models using Soleus signals consistently performing best.

The average number of epochs until termination increased from 30 to 35. Fig. 8 illustrates the combination specific performance when not using additional spatial samples compared when the regularization is applied, visualized on the grid. This shows an increased robustness to longitudinal shifts compared to lateral ones, a pattern observed in all subjects and muscle groups in these results.
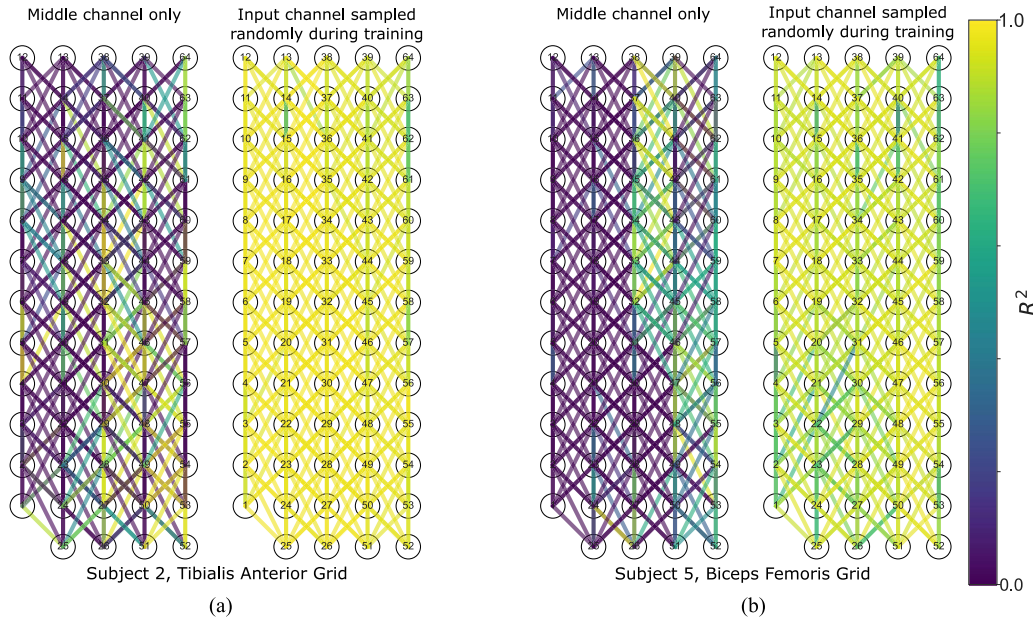
Fig. 8. R^2 performance of models evaluated on every valid electrode combination on a grid, shown for TA in participant 2 (a), and BF in participant 5 (b). The left grid in each panel shows models that were only trained with the middle combination (31–33). The right grid in each panel shows performance if the input electrode combinations are sampled uniformly during training. R^2 values are visualized with a lower limit of 0. Transparent lines are used, as the region of interest for each electrode contains overlapping sections (see collinear combinations in Fig. 2).
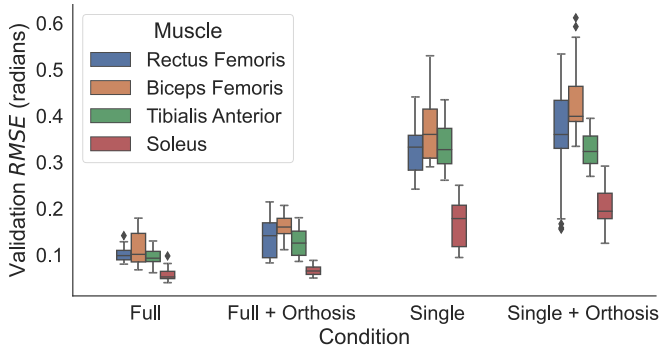

Fig. 9. Predicted knee angle RMSE of each muscle group across conditions when trained on the entire grid (Full) versus only the SENIAM bipolar combination in the centre of the grid (single). The condition of wearing the knee orthosis is also shown.
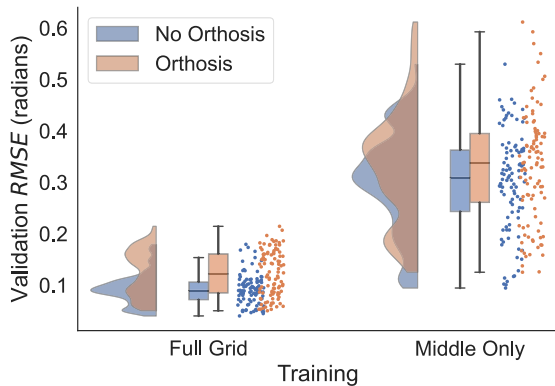

Fig. 10. Average model performance across all valid bipolar combinations of the grid. Models were trained either with electrode combinations sampled uniformly from the grid, or solely with the middle combination (electrodes 31 and 33). The hue determines whether the model was trained and evaluated with data recorded while wearing a knee orthosis.
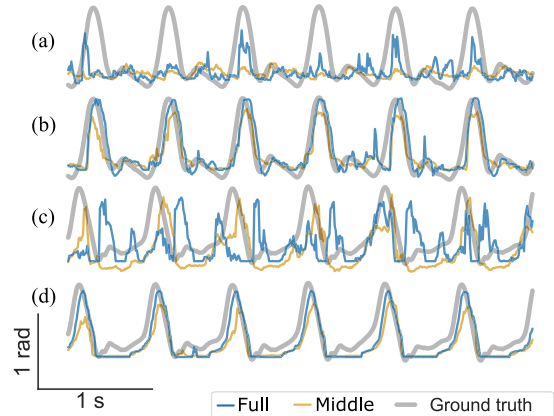

Fig. 11. Knee flexion predictions with data recorded with Delsys bipolar electrode, with models trained on signal from the HD-sEMG grid. Two subjects shown, subject 3 with the RF (a) and TA (b), and subject 1 with the BF (c) and SO (d). "Full" refers sampling the input channel uniformly from the entire grid, "Middle" refers to only training with the middle location. The angle from motion capture is overlaid.

IV. DISCUSSION

Our chosen consistency metrics were validated as indicators of signal quality, since electrode locations selected through them were associated with higher prediction accuracy, when compared to those hand-aligned based on guidelines. This suggests that consistency metrics could be used for high-level analysis of signal quality, especially in models with short input windows. However, no distinct pattern emerged to reliably identify better areas on the skin surface for sEMG acquisition from a given muscle. Not only was there no clear preferred electrode position
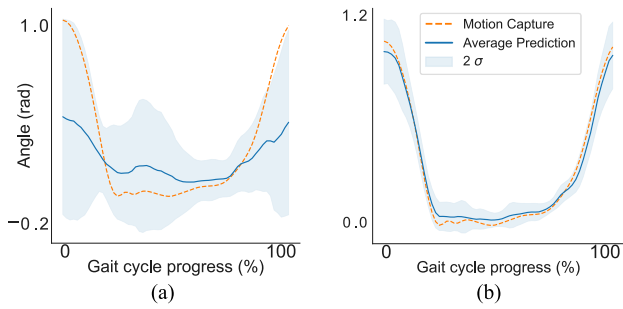
Fig. 12. Standard deviation of the average gait cycle across electrode combinations for the BF models of participant 4. (a) The average prediction of a model trained with just the middle sampling, showing that the uncertainty is phase dependent. (b) The average prediction from a model trained with combinations across the grid.
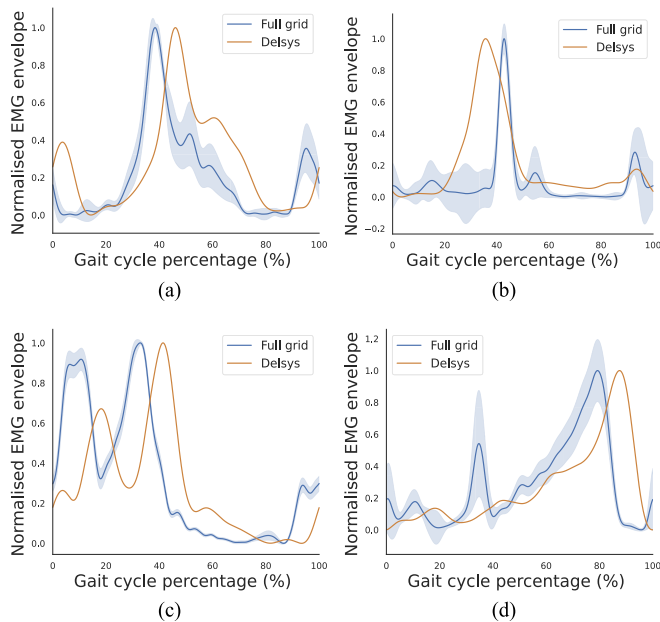

Fig. 13. Comparison of the average bipolar sEMG signal envelopes across the HD-sEMG grid with the bipolar signals from the Delsys system for (a) the RF, (b) the BF, (c) the TA, and (d) the SO. The HD-sEMG error band corresponds to the spatial variation of the signal.

on the muscle, but even small electrode shifts caused significant prediction accuracy degradation. Due to the severe impact of electrode shifts, and the inevitable placement discrepancies between sessions from electrode reapplication [42], relying on optimal electrode placement is unrealistic. We must therefore prioritize the development of spatially robust models to improve gait prediction for exoskeleton applications. As the signal feature landscape is heavily affected by interference from the orthosis (Fig. 7), including this condition should be a high priority for future studies investigating signal acquisition for neuroorthoses. Potential causes for this difference may involve the additional stress, shear and relative movement at the orthosis-electrode grid interface. Alternate causes may originate from a change in the muscle activity due to the additional weight or DoF restriction. Lastly, a phase shift may be caused by the replacement of the motion capture markers, necessitated by the orthosis. However, since on Fig. 7(c) the effect is nonuniform, this does not appear to

be the dominant cause. Mitigating these effects through orthosis design and fitting could be investigated for more reliable signal acquisition.

The use of spatial correlations in sEMG signals can significantly improve robustness [43], however, the generalization of spatially rich HD-sEMG data for bipolar applications has not yet been investigated. Increasing the size of the electrode detection surface helps reducing model sensitivity to electrode shifts when perpendicular to the muscle fibres [18]. Hence, it can be hypothesized that increasing the data acquisition area from an electrode grid would improve model robustness in a similar way.

By collecting data from all 360 possible bipolar locations across the model, we widened the training data distribution to include more possible scenarios that could be encountered due to electrode shifts. A wider range of spatial samplings includes channels where the effect of physiological features, such as muscle cross-talk and innervation zone (IZ) effects, manifest to different extents. As such, this could promote the recognition and reduction of these sources by the model, leading to more stable predictions. Another possibility is that modeling multiple orientations encourages the TCN to favor features that are on a longer time-scale, and are shared across various channels. This group training approach has been met with scepticism in the past, as it was previously associated with longer acquisition and signal processing times [44]. However, these concerns were partly addressed in this study with the simultaneous collection of bipolar signals through the grid and the sampling of electrode location during training. A further limitation of the group training approach is that the additional training information can potentially crowd the feature space and decrease model performance for the original nonshifted location [20]. Whilst it is true that spatial sampling methods decrease the average maximum performance, this regularization method can still be a useful tool in training models, especially in scenarios where electrode shifts are inevitable. Within an exoskeleton context, due to its dynamic application to the lower-limbs, model robustness needs to be prioritized, and performance degradation can be moderated by other components in the system such as a higher-level controller or sensor fusion techniques [8], [45]. Furthermore, using grid recordings to train spatially generalising models could facilitate muscle selection studies by removing the impact of specific electrode placement on signal quality, and allowing for a more general comparison of signal reliability across muscles (see Fig. 9).

Including bipolar samplings from across the grid does not substantially increase the training time of the predictive network, making this method convenient during both data acquisition and processing. Defining a nonuniform sampling distribution may allow the tradeoff of generalization and maximum performance to be fine-tuned. The observation that longitudinal shifts lead to less decline in performance is congruent with existing work [22]. Movements perpendicular to muscle fibres correspond to locations influenced by different neighboring muscles, or to areas with different neurophysiological characteristics, such as the anterior aspect of the tibia. Fig. 12(a) exhibits a heteroskedastic distribution throughout the gait cycle, which further illustrates

the nonlinearity of the signal variation across channels. However, our approach enabled the TCN to be robust to these transformations and phase shifts, as illustrated in Fig. 12(b).

Despite many differences, such as electrode size, original sampling frequency, and the use of electrode gel in the grid, there is a potential for transferability of information across acquisition systems. This would enable rapid and spatially rich data collection from grids utilized for robust bipolar applications. The shift in the profiles of the Delsys signals relative to the simulated bipolar signals from HD-sEMG, and the failure of the model transfer in the case of the thigh muscles (Fig. 11) would suggest that this regularization method would likely have to be combined with domain adaptation techniques to fine-tune predictions to various expected conditions [46]. Furthermore, this method does not necessarily mitigate the requirement to recalibrate networks due to long-term changes in the neural interface, or application to different subjects. The combined application of the different frameworks addressing these key issues should be investigated [47].

The approach of deploying pretrained models may not be as effective in cases where the signal is subjected to external disturbances not accounted for during training; wearing an orthosis, changing speed, electromagnetic interference, electrode reapplication, sweating, or fatigue [4], [48]. To account for the signal alterations caused by external factors, data augmentation approaches, including nonlinear transformations of the training set, are promising. This would require in-depth analysis of the impact of different environmental factors to reproduce them into the training distribution, which could be accelerated by the acquisition of spatially robust features.

Steady-state level ground walking was selected as target motion as it facilitated the efficient collection of many repetitions of the same movement. However, the intended movement is not without variation. A degree of variability is present in the dependent variable due to small changes in gait patterns adopted by the participants over the course of a trial. A well performing model must be able to track these effects. This is a limitation of the described consistency metrics, as they do not distinguish between meaningful, informative variability and noise. A nonsteady-state locomotion setting, including transitions such as turning or coming to a stop would be suitable to explore the intent estimation aspect further.

Increasing the size of the input window led to an increase in performance and a decrease in the sensitivity to specific electrode placements (Fig. 6). However, longer input intervals imply greater computational cost both during training and inference, making the optimal window size vary depending on the requirements of a given application. The impact of this parameter on the model's sensitivity to intent changes in particular should be examined. Lastly, in addition to the window size, the influence of other TCN hyperparameters on prediction stability should be investigated.

V. Conclusion

The investigated consistency metrics were validated as indicators of signal quality, with the selected samples leading to higher output accuracy from the TCN. This correlation could be used to identify electrode placements that will perform better in data-driven models. However covariate shifts due to changing conditions and variability in intersession electrode replacement makes optimizing for a single, high signal quality location unreliable. The use of HD-sEMG grids for data acquisition with the aim of bipolar applications enables the inclusion of valuable spatial information that improves model robustness to electrode shifts. While there appears to be transferability between HD-sEMG and bipolar sEMG signals, future works should focus on domain transfer methods to seamlessly reproduce bipolar signals from HD-sEMG grids, and construct data augmentation strategies based on expected distributional shifts for all deployment environments. Current work involves applying these findings to lower-limb exoskeletons in order to achieve robust AAN control.

References

[1] K. Knaepen, P. Beyl, S. Duerinck, F. Hagman, D. Lefeber, and R. Meeusen, "Human-robot interaction: Kinematics and muscle activity inside a powered compliant knee exoskeleton," *IEEE Trans. Neural Syst. Rehabil. Eng.*, vol. 22, no. 6, pp. 1128–1137, Nov. 2014.

[2] D. Staudenmann, K. Roeleveld, D. F. Stegeman, and J. H. van Dieën, "Methodological aspects of sEMG recordings for force estimation–a tutorial and review," *J. Electromyogr. Kinesiol.*, vol. 20, no. 3, pp. 375–387, 2010.

[3] C. Caulcrick, W. Huo, W. Hoult, and R. Vaidyanathan, "Model predictive control for human-centred lower limb robotic assistance," *IEEE Trans. Med. Robot. Bionics*, vol. 3, no. 4, pp. 980–991, Nov. 2021.

[4] M. A. Oskoei and H. Hu, "Myoelectric control systems–a survey," *Biomed. Signal Process. Control*, vol. 2, no. 4, pp. 275–294, 2007.

[5] B. Sheng, L. Tang, S. Xie, C. Deng, and Y. Zhang, "Alterations in muscle activation patterns during robot-assisted bilateral training: A pilot study," *Proc. Inst. Mech. Engineers. Part H., J. Eng. Med.*, vol. 233, no. 2, pp. 219–231, Feb. 2019.

[6] R. Jimenez-Fabian and O. Verlinden, "Review of control algorithms for robotic ankle systems in lower-limb orthoses, prostheses, and exoskeletons," *Med. Eng. Phys.*, vol. 34, no. 4, pp. 397–408, 2012.

[7] C. R. Steinhardt, J. Bettthauser, C. Hunt, and N. Thakor, "Registration of EMG electrodes to reduce classification errors due to electrode shift.," in *Proc. IEEE Biomed. Circuits Syst. Conf.*, 2018, pp. 1–4.

[8] M. R. Tucker et al., "Control strategies for active lower extremity prosthetics and orthotics: A review," *J. Neuroengineering Rehabil.*, vol. 12, no. 1, pp. 1–30, 2015.

[9] B. Rodríguez-Tapia, I. Soto, D. M. Martínez, and N. C. Arballo, "Myoelectric interfaces and related applications: Current state of EMG signal processing–a systematic review," *IEEE Access*, vol. 8, pp. 7792–7805, 2020.

[10] M. Simao, N. Mendes, O. Gibaru, and P. Neto, "A review on electromyography decoding and pattern recognition for human-machine interaction," *IEEE Access*, vol. 7, pp. 39564–39582, 2019.

[11] D. Xiong, D. Zhang, X. Zhao, and Y. Zhao, "Deep learning for EMG-based human-machine interaction: A review," *IEEE/CAA J. Automatica Sinica*, vol. 8, no. 3, pp. 512–533, Mar. 2021.

[12] I. Campanini, A. Merlo, P. Degola, R. Merletti, G. Vezzosi, and D. Farina, "Effect of electrode location on EMG signal envelope in leg muscles during gait," *J. electromyogr. kinesiol.*, vol. 17, no. 4, pp. 515–526, 2006.

[13] A. Subbaswamy and S. Saria, "From development to deployment: Dataset shift, causality, and shift-stable models in health AI," *Biostatistics*, vol. 21, no. 2, pp. 345–352, 2020.

[14] H. J. Hermens et al., "European recommendations for surface electromyography," *Roessingh Res. Develop.*, vol. 8, no. 2, pp. 13–54, 1999.

[15] R. Merletti and S. Muceli, "Tutorial. surface EMG detection in space and time: Best practices," *J. electromyogr. kinesiol.*, vol. 49, Dec. 2019, Art. no. 102363.

[16] A. Rainoldi, G. Melchiorri, and I. Caruso, "A method for positioning electrodes during surface EMG recordings in lower limb muscles," *J. Neurosci. Methods*, vol. 134, no. 1, pp. 37–43, 2004.

[17] I. C. N. Sacco, A. A. Gomes, M. E. Otuzi, D. Pripas, and A. N. Onodera, "A method for better positioning bipolar electrodes for lower limb EMG recordings during dynamic contractions," *J. Neurosci. Methods*, vol. 180, no. 1, pp. 133–137, 2009.

[18] A. J. Young, L. J. Hargrove, and T. A. Kuiken, "The effects of electrode size and orientation on the sensitivity of myoelectric pattern recognition systems to electrode shift," *IEEE Trans. Biomed. Eng.*, vol. 58, no. 9, pp. 2537–2544, Sep. 2011.

[19] X. Zhang, L. Wu, B. Yu, X. Chen, and X. Chen, "Adaptive calibration of electrode array shifts enables robust myoelectric control," *IEEE Trans. Biomed. Eng.*, vol. 67, no. 7, pp. 1947–1957, Jul. 2020.

[20] J. He, X. Sheng, X. Zhu, and N. Jiang, "Position identification for robust myoelectric control against electrode shift," *IEEE Trans. Neural Syst. Rehabil. Eng.*, vol. 28, no. 12, pp. 3121–3128, Dec. 2020.

[21] J. He, X. Sheng, X. Zhu, and N. Jiang, "A novel framework based on position verification for robust myoelectric control against sensor shift," *IEEE Sensors J.*, vol. 19, no. 21, pp. 9859–9868, Nov. 2019.

[22] A. J. Young, L. J. Hargrove, and T. A. Kuiken, "Improving myoelectric pattern recognition robustness to electrode shift by changing interelectrode distance and electrode configuration," *IEEE Trans. Biomed. Eng.*, vol. 59, no. 3, pp. 645–652, Mar. 2012.

[23] L. Wu, X. Zhang, K. Wang, X. Chen, and X. Chen, "Improved high-density myoelectric pattern recognition control against electrode shift using data augmentation and dilated convolutional neural network," *IEEE Trans. Neural Syst. Rehabil. Eng.*, vol. 28, no. 12, pp. 2637–2646, Dec. 2020.

[24] C. Lea, M. D. Flynn, R. Vidal, A. Reiter, and G. D. Hager, "Temporal convolutional networks for action segmentation and detection," in *Proc. IEEE Conf. Comput. Vis. Pattern Recognit.*, 2017, pp. 156–165.

[25] S. Bai, J. Z. Kolter, and V. Koltun, "An empirical evaluation of generic convolutional and recurrent networks for sequence modeling," 2018, *arXiv:1803.01271*.

[26] B. Fang et al., "Gait neural network for human-exoskeleton interaction," *Front. Neurorobot.*, vol. 14, 2020, Art. no. 58.

[27] I. Kang, D. D. Molinaro, S. Duggal, Y. Chen, P. Kunapuli, and A. J. Young, "Real-time gait phase estimation for robotic hip exoskeleton control during multimodal locomotion," *IEEE Robot. Automat. Lett.*, vol. 6, no. 2, pp. 3491–3497, Apr. 2021.

[28] J. Liu, C. Wang, B. He, P. Li, and X. Wu, "Metric learning for robust gait phase recognition for a lower limb exoskeleton robot based on sEMG," *IEEE Trans. Med. Robot. Bionics*, vol. 4, no. 2, pp. 472–479, May 2022.

[29] H. Huang, P. Zhou, G. Li, and T. A. Kuiken, "An analysis of EMG electrode configuration for targeted muscle reinnervation based neural machine interface," *IEEE Trans. Neural Syst. Rehabil. Eng.*, vol. 16, no. 1, pp. 37–45, Feb. 2008.

[30] OT Bioelettronica, "Otbiolab user manual v3.4," 2022. Accessed Jan. 19, 2022. [Online]. Available: https://www.otbioelettronica.it/files/47/Software/15/OTBioLab-User-Manual-ENG.pdf

[31] E. S. Grood and W. J. Suntay, "A joint coordinate system for the clinical description of three-dimensional motions: Application to the knee," *J. Biomechanical Eng.*, vol. 105, no. 2, pp. 136–144, 1983.

[32] C. L. Vaughan, B. L. Davis, and J. C. O'connor, *Dynamics of Human Gait*, vol. 2. Champaign, IL, USA: Human Kinetics, 1992.

[33] B. G. Lapatki, R. Oostenveld, J. P. V. Dijk, I. E. Jonas, M. J. Zwarts, and D. F. Stegeman, "Optimal placement of bipolar surface EMG electrodes in the face based on single motor unit analysis," *Psychophysiology*, vol. 47, no. 2, pp. 299–314, Mar. 2010.

[34] A. Burden, "How should we normalize electromyograms obtained from healthy participants? What we have learned from over 25 years of research," *J. Electromyogr. Kinesiol.*, vol. 20, no. 6, pp. 1023–1035, 2010.

[35] M. Zanghieri, S. Benatti, A. Burrello, V. Kartsch, F. Conti, and L. Benini, "Robust real-time embedded EMG recognition framework using temporal convolutional networks on a multicore IoT processor," *IEEE Trans. Biomed. Circuits Syst.*, vol. 14, no. 2, pp. 244–256, Apr. 2020.

[36] J. L. Betthauser et al., "Stable responsive EMG sequence prediction and adaptive reinforcement with temporal convolutional networks," *IEEE Trans. Biomed. Eng.*, vol. 67, no. 6, pp. 1707–1717, Jun. 2020.

[37] T. G. Dietterich, "Approximate statistical tests for comparing supervised classification learning algorithms," *Neural Comput.*, vol. 10, no. 7, pp. 1895–1923, 1998.

[38] F. Sylos-Labini et al., "Emg patterns during assisted walking in the exoskeleton," *Front. Hum. Neurosci.*, vol. 8, Jun. 2014, Art. no. 423.

[39] J. M. Hidler and A. E. Wall, "Alterations in muscle activation patterns during robotic-assisted walking," *Clin. Biomech.*, vol. 20, no. 2, pp. 184–193, 2005.

[40] R. G. Mello, L. F. Oliveira, and J. Nadal, "Digital butterworth filter for subtracting noise from low magnitude surface electromyogram," *Comput. Methods Programs Biomed.*, vol. 87, no. 1, pp. 28–35, 2007.

[41] F. Chollet et al., "Keras," 2015. [Online]. Available: https://keras.io

[42] G. S. Murley, H. B. Menz, K. B. Landorf, and A. R. Bird, "Reliability of lower limb electromyography during overground walking: A comparison of maximal- and sub-maximal normalisation techniques," *J. Biomech.*, vol. 43, no. 4, pp. 749–756, 2009.

[43] A. Stango, F. Negro, and D. Farina, "Spatial correlation of high density EMG signals provides features robust to electrode number and shift in pattern recognition for myocontrol," *IEEE Trans. Neural Syst. Rehabil. Eng.*, vol. 23, no. 2, pp. 189–198, Mar. 2015.

[44] S. Kyeong and J. Kim, "Enhanced torque estimation method from multi-channel surface electromyography compensating electrode location variation," in *Proc. 42nd Annu. Int. Conf. IEEE Eng. Med. Biol. Soc.*, 2020, pp. 3965–3968.

[45] J. Camargo, W. Flanagan, N. Csomay-Shanklin, B. Kanwar, and A. Young, "A machine learning strategy for locomotion classification and parameter estimation using fusion of wearable sensors," *IEEE Trans. Biomed. Eng.*, vol. 68, no. 5, pp. 1569–1578, May 2021.

[46] A. Ameri, M. A. Akhaee, E. Scheme, and K. Englehart, "A deep transfer learning approach to reducing the effect of electrode shift in EMG pattern recognition-based control," *IEEE Trans. Neural Syst. Rehabil. Eng.*, vol. 28, no. 2, pp. 370–379, Feb. 2020.

[47] K.-T. Kim, C. Guan, and S.-W. Lee, "A subject-transfer framework based on single-trial EMG analysis using convolutional neural networks," *IEEE Trans. Neural Syst. Rehabil. Eng.*, vol. 28, no. 1, pp. 94–103, Jan. 2020.

[48] G. Venugopal, M. Navaneethakrishna, and S. Ramakrishnan, "Extraction and analysis of multiple time window features associated with muscle fatigue conditions using sEMG signals," *Expert Syst. Appl.*, vol. 41, no. 6, pp. 2652–2659, 2014.